https://doi.org/10.1016/j.jsv.2023.118019

Design optimization of a single-mass impact damper

Muhammad Ayaz AKBAR[1], Wai On WONG[1*], Emiliano RUSTIGHI[2]

[1]*Department of Mechanical Engineering, The Hong Kong Polytechnic University, Hong Kong SAR*
[2]*Department of Industrial Engineering, University of Trento, Trento, Italy*

Abstract

This research article presents a numerical approach to establish an optimal design methodology for a single-mass impact damper (SMID), which is a passive energy dissipation device with robust performance. Due to the nonlinear characteristics of SMID and a lack of analytical models, designing a single-mass impact damper with optimal combination of the parameters has been challenging. Furthermore, an uncontrolled mass of the SMID on a vibrating structure may lead to chaotic vibration responses. This study identifies a range of design parameters of the SMID to ensure non-chaotic responses and validates the optimal design combinations using an experimental prototype. The results show that a single-mass impact damper designed with the optimal combination of design parameters can provide better vibration damping and relatively steady response. This study also compares the performance of an optimized single-mass impact damper with an optimized tuned mass damper and finds that the single-mass impact damper can work more effectively than the tuned mass damper in damping free vibrations of a single-degree-of-freedom primary structure. Although the SMID cannot suppress forced vibration amplitude as effectively as a tuned mass damper (TMD) at resonance, it has the advantages of lower cost and easier installation than the TMD. Overall, this study provides a basis for the optimal design of a single-mass impact damper and resolves the issues related to design methodology and chaotic vibration response with a single-mass impact damper.

Keywords*: Single-mass impact damper; Particle impact damper; Passive vibration control; Optimal design; Tuned Mass Damper.*

[*] Corresponding author.

E-mail address: mmwowong@polyu.edu.hk (Wai On Wong)

Nomenclature

Symbols	
$\ddot{\mathbf{x}}$	Acceleration of primary structure; m/s^2
$\ddot{\mathbf{y}}$	Acceleration of particle; m/s^2
$\mathbf{Z}$	Amplitude of ground motion; m
$\mathbf{d}$	Clearance; m
$\mathbf{e}$	Coefficient of restitution;
$\mathbf{c}$	Damping coefficient; Ns/m
$\boldsymbol{z}$	Displacement of support; m
$\mathbf{y}$	Displacement of particle; m
$\mathbf{x}$	Displacement of primary structure; m
$\mathbf{F(t)}$	Excitation force; N
$\mathbf{x_0}$	Initial position of primary structure; m
$\mathbf{y_0}$	Initial position of particle; m
$\dot{\mathbf{x}}_\mathbf{0}$	Initial velocity of primary structure; m/s
$\dot{\mathbf{y}}_\mathbf{0}$	Initial velocity of particle; m/s
$\mathbf{M}$	Mass of primary structure; kg
$\mathbf{m}$	Mass of primary structure; kg
$\mathbf{k}$	Spring constant; N/m
$\dot{\boldsymbol{z}}$	Velocity of support; m/s
$\dot{\mathbf{y}}$	Velocity of particle; m/s
$\dot{\mathbf{x}}$	Velocity of primary structure; m/s
$\dot{\mathbf{y}}_\mathbf{n}^+$	Velocity of particle after n^{th} impact; m/s
$\dot{\mathbf{y}}_\mathbf{n}^-$	Velocity of particle before n^{th} impact; m/s
$\dot{\mathbf{x}}_\mathbf{n}^+$	Velocity of primary structure after n^{th} impact; m/s
$\dot{\mathbf{x}}_\mathbf{n}^-$	Velocity of primary structure before n^{th} impact; m/s
Greek Symbols	
$\boldsymbol{\mu_i}$	Coefficient of friction (Internal Friction friction);
$\boldsymbol{\omega}$	Frequency of excitation force; rad/s
$\boldsymbol{\gamma_g}$	Friction force ratio related to ground disturbance;
$\boldsymbol{\omega_n}$	Natural frequency of primary structure; rad/s
$\boldsymbol{\beta}$	Mass ratio; m/M
Abbreviations	
SMID	Single-mass impact damper
PID	Particle Impact Damper
RMS	Root Mean Square.
FD	Friction damper
SDOF	Single degree of freedom
TMD	Tuned Mass Damper

1. Introduction

Single-mass impact damper (SMID) is a passive vibration damper for reducing the response of the structures under excitations. SMID can be considered as a special type of particle impact damper (PID) with only one particle mass in the cavity [1]. Moreover, most of the studies on particle dampers assume various particles as a single mass in the theoretical analysis due to complex nonlinearities associated with multiparticle dampers [2-8]. Based on the number of particles in the cavity, it can be classified into single-mass impact damper or multiparticle damper. The dissipation of the vibration energy occurs through impacts and momentum exchange between the primary mass and particle [9]. They are equally effective in harsh conditions and their simple installation process, less sensitivity to the direction of excitation [10], and various other benefits make them favourable over other passive and semi-active damping technologies [11]. In addition to that, SMIDs are negligibly sensitive to oil contamination, do not add excessive external weight [1], and are usually insensitive to atmospheric temperature [12]. SMIDs are very efficient at damping several kinds of excitations [13] (e.g., excitations by impacts, and random excitations). Wear is less likely to happen in SMIDs [12], and are simple, affordable, and highly reliable devices [14] used for vibration control. A key aspect of single-mass impact dampers is that they can operate in multiple directions and at a wide range of frequencies [15]. Recent evidence suggests that single-mass impact dampers can be explicitly designed to be less sensitive to excitations other than the principle direction [16]. Therefore, they have been frequently studied and applied in the area of vibration control in aviation, machinery and structures [17-22].

The study of single-mass impact dampers can be tracked back from the research of Lieber et al [23] in 1945, where it was assumed that every impact between particle and primary structure is a perfect plastic collision and the working principle of SMID follows momentum exchange and friction between the particle and primary structure. However, Grubin [24] disagree with the assumption and proposed a theoretical model with a recovery coefficient (coefficient of restitution) with inelastic impacts. Later, Masri [25, 26] presented an analytical expression for steady-state vibration of a single-degree-of-freedom structure with a single-mass impact damper under harmonic excitations. It was concluded that the theoretical model of the traditional single-mass impact damper is highly nonlinear, therefore, the analytical solution is only possible under the assumption of two symmetric impacts per cycle and steady-state vibrations. However, these assumptions are not true in practice. Therefore, numerical simulations are performed on the model of a single-mass impact damper for a better connection with theoretical and experimental

results. Additionally, various experimental studies have been conducted on single-mass impact dampers. Li et al [27, 28] presented the effects of different parameters on the damping performance of single-mass impact dampers with shaking table tests on a three-story frame structure. The results revealed that the first vibration mode of the multi-story structure is damped effectively, however, the effectiveness of a single-mass impact damper on the higher vibration modes is not guaranteed, and the cavity length is a crucial parameter for SMID design. Hossein [29] presented an experimental and analytical study of a single-single-mass impact damper in free vibrations. It was concluded that the friction between the particle and primary structure degrades the damping in free vibrations due to the reduced velocity of the particle because of friction. Yiqing et al [30] presented a study for the optimal parameters of a single-mass impact damper embedded on a cantilever beam considering its velocity response, and it was concluded that reverse-direction collision produces higher damping than co-directional collision. Duncan et al [31] presented a numerical analysis of the damping performance of a single-single-mass impact damper in the vertical direction. It was concluded that the clearance magnitude is cruicial prameter and the optimal clearance increases with the increase in mass ratio and main structure's damping ratiobut decreases with coefficeint of restitution.

In contrast, multiparticle dampers generally contain multiple small particles in a cavity attached to the primary structure [32]. The working principle of multiparticle dampers is similar to the single-mass impact damper, where energy is dissipated through impacts and momentum exchange between primary mass and particles. However, a multiparticle damper can dissipate the vibration energy of the primary system through particle-particle impacts as well [33-35]. Despite showing practical advantages over SMID, the design methodology of a multiparticle damper is highly challenging due to complex nonlinearities. The uneven clearance magnitude and complicated interactions between particles make it difficult to predict the actual response and formulate a reliable design method [36]. Therefore, most of the studies found in the literature are valid for a specific case and are conducted based on trial and error. Few studies predicting a design methodology consider a multiparticle damper as a single-mass impact damper for numerical analysis. Consequently, it is reported that a multiparticle damper shows good damping but multiple particles in the damper cavity restrict their effective movement leading to a decreased momentum exchange between particles and primary mass [37, 38]. Therefore, it is necessary to optimize the design methodology of the single-mass impact damper to achieve better agreement between theory and practice.

Single-mass impact dampers are known as nonlinear devices where a general optimal design method is challenging to develop due to complicated nonlinear relationships between parameters. However, this study presents a design methodology for a single-mass impact damper in free and forced (harmonic) vibrations considering all the critical design parameters and their relationships. A numerical model is established to simulate the performance of the single-mass impact damper over various design combinations. The numerical model is used to obtain a range of optimal combinations for a single-mass impact damper design in free and forced vibrations. Moreover, friction between the motion of the particle is considered an important parameter for the optimal design. Therefore, the numerical model presented in this study includes internal friction for more practical results. Overall, experimental results are consistent with the numerical approach, verifying the accuracy of the results. Earlier research about SMID considered one parameter at a time to find an optimum range for the specific parameter, however, this study shows that the major design parameters of single-mass impact damper are correlated. Therefore, it is necessary to formulate an optimal range while considering more than one parameter at once. This study considers major design parameters simultaneously for an optimum design of a single-mass impact damper for the very first time. Additionally, a tuning range of major design parameters for the single-mass impact damper is established for any harmonic excitation. Furthermore, it is observed that the chaotic response of the primary structure is a possibility if the single-mass impact damper is used without prior understanding. Therefore, a range of parameters with a relatively non-chaotic response is determined with the help of a Poincare map. Overall, an effective single-mass impact damper can be designed by following the methodology presented in this study for any free and forced (harmonic) vibration application.

2. Numerical model and computation process

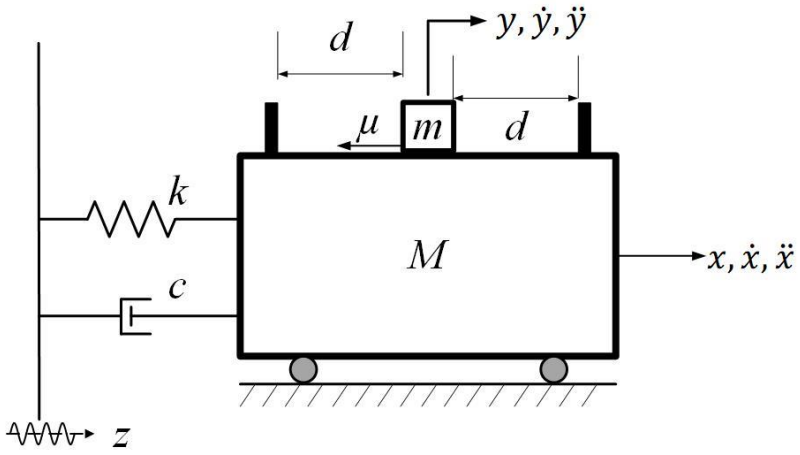

Fig. 1. The mechanical model of a single-mass impact damper attached to the SDOF structure.

The mechanical model of the SDOF structure associated with a single-mass impact damper is shown in Fig. 1. The mass of the primary structure is M, while the mass of the particle is denoted as m. The particle can travel within a distance $2d$ and hit the primary structure when it reaches the boundary. The equation of motion for the primary structure with friction between the particle and primary mass relative motion can be written as,

$$M\ddot{x} + c(\dot{x} - \dot{z}) + k(x - z) + \mu_i N_m \operatorname{sgn}(\dot{x} - \dot{y}) = 0 \tag{1}$$

The equation of motion for the particle can be written as,

$$m\ddot{y} = \mu_i N_m \operatorname{sgn}(\dot{x} - \dot{y}) \tag{2}$$

Here μ is the coefficient of friction between the particle and primary mass. $N_m = mg$ is the weight of particle mass, and sgn represents the signum function which defines the direction of the friction force. The signum function, in this case, is defined as,

$$\operatorname{sgn}(\dot{x} - \dot{y}) = \begin{cases} -1, & (\dot{x} - \dot{y}) < 0 \\ 0, & (\dot{x} - \dot{y}) = 0 \\ 1, & (\dot{x} - \dot{y}) > 0 \end{cases} \tag{3}$$

The equation of conservation of momentum for two colliding bodies is written as

$$M\dot{x}_n^- + m\dot{y}_n^- = M\dot{x}_n^+ + m\dot{y}_n^+ \tag{4}$$

where $(\dot{x}_n^+, \dot{x}_n^-)$ are the velocities of the primary structure before and after n^{th} impact. The superscript $(+)$ denotes the velocity after impact and $(-)$ denotes the velocity before impact. Similarly, $(\dot{y}_n^+, \dot{y}_n^-)$ denotes the velocities of particles before and after (n^{th}) impact.

Energy is dissipated at each collision depending on the magnitude of the coefficient of restitution, *e*, defined as,

$$e = -\frac{\dot{x}_n^+ - \dot{y}_n^+}{\dot{x}_n^- - \dot{y}_n^-} \tag{5}$$

The change in velocities of the primary structure and the particle after each impact depends on both momentum exchange and energy dissipation. Physically, the coefficient of restitution may be used to determines the energy dissipation at each impact due to the deforming of the impact surface, sound, and heat. It can be shown that when $e = 1$, there is no energy dissipation and maximum momentum exchange between the bodies depending on the direction of motion and

mass difference. In contrast, maximum kinetic energy is absorbed during the impact, and minimum momentum exchange between the impacting bodies when $e = 0$.

Combining and rearranging Eqs. (4) and (5) for the velocities of particle and primary structure after each impact gives,

$$\dot{x}_n^+ = \frac{[\{(1-\beta e)\dot{x}_n^-\} + \{\beta(1+e)\dot{y}_n^-\}]}{(1+\beta)} \tag{6}$$

$$\dot{y}_n^+ = \frac{[\{(1+e)\dot{x}_n^-\} + \{(\beta-e)\dot{y}_n^-\}]}{(1+\beta)} \tag{7}$$

Here β is the mass ratio and is calculated as $\beta = \frac{m}{M}$. These equations are used to determine the velocities after each impact. The condition for determining an impact is stated in Equation (8). Making use of the absolute difference between *x* and *y*, the impact on either end surface of the SMID can be determined.

$$|x(t) - y(t)| \geq d \tag{8}$$

The flowchart in Fig. 2 shows the computation principle of the dynamic motions of the model in Fig. 1. The process begins with the vibration of the primary structure due to an initial condition (x_0, $\dot{x}_0$) or support motion, $z(t)$. The impact in the SMID is then identified based on the condition ($|x(t) - y(t)| > d$). The velocities of masses *M* and *m* after the impacts are calculated using Eqs. (6) and (7). Then the computation restarts based on the calculated velocities and the position of the two masses after the time of impact as initial conditions. If the condition for the impact is not satisfied, then the next time step is computed. A minimum time step is recommended for determining the precise impact time, although it may increase the computational effort.

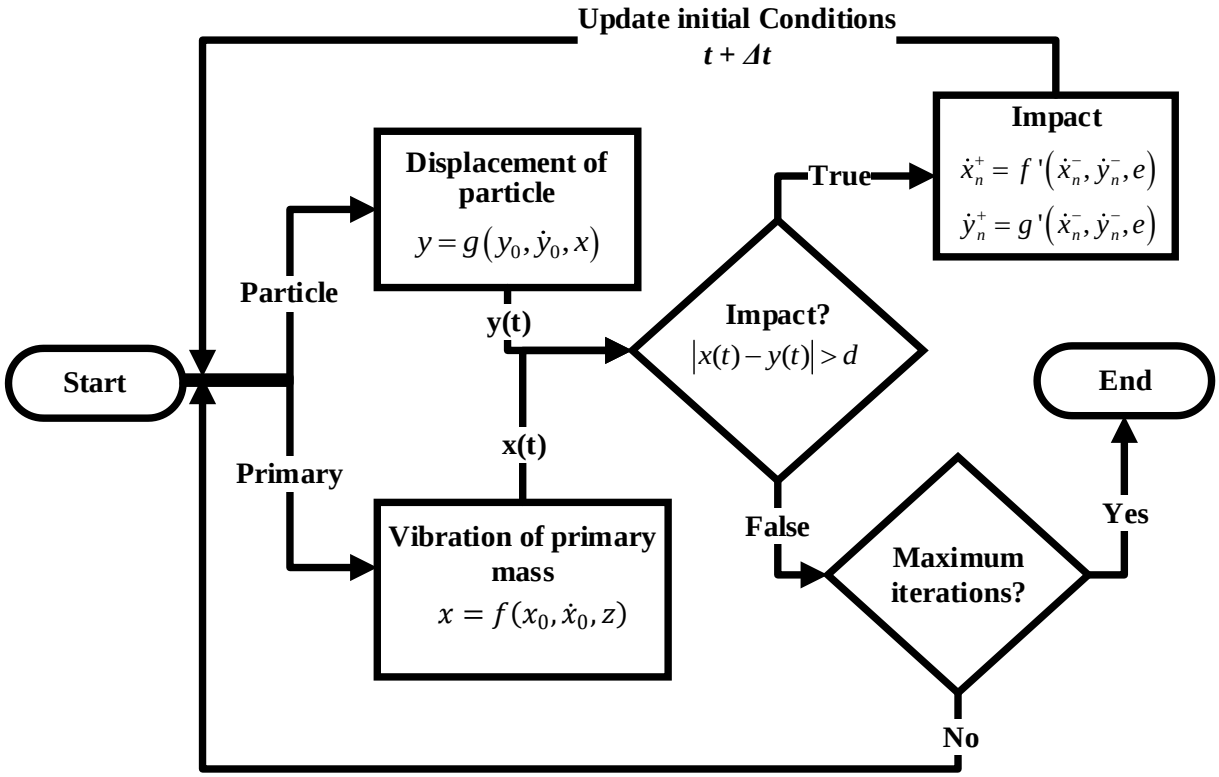

Fig. 2. Process flow chart of the numerical model.

Generally, the design parameters for the design of single-mass impact dampers are clearance *d*, coefficient of restitution *e*, and mass ratio β [39, 40]. Even though the fundamental design parameters are well known, the optimal design approaches are underdeveloped due to the nonlinear correlations of these parameters. In addition to the mentioned design parameters, also the friction in the motion of the particle is considered in this study. Friction is present in all mechanical systems, therefore, analyzing the performance of a single-mass impact damper with friction can formulate more practical conclusions. It is well understood that the working principle of a single-mass impact damper is based on the impact between the primary system and particles, and the velocity of the particle plays a major role in determining the dynamics of the primary structure after each impact.

2.1. Tuned Mass Damper (TMD)

A traditional tuned mass damper (TMD) is a passive vibration absorbing device which is pre-tuned to a particular frequency as shown in Fig. 3. TMD is a widely researched vibration absorber with considerable knowledge of analytical methods for its optimal design for maximum vibration suppression of the primary structure.

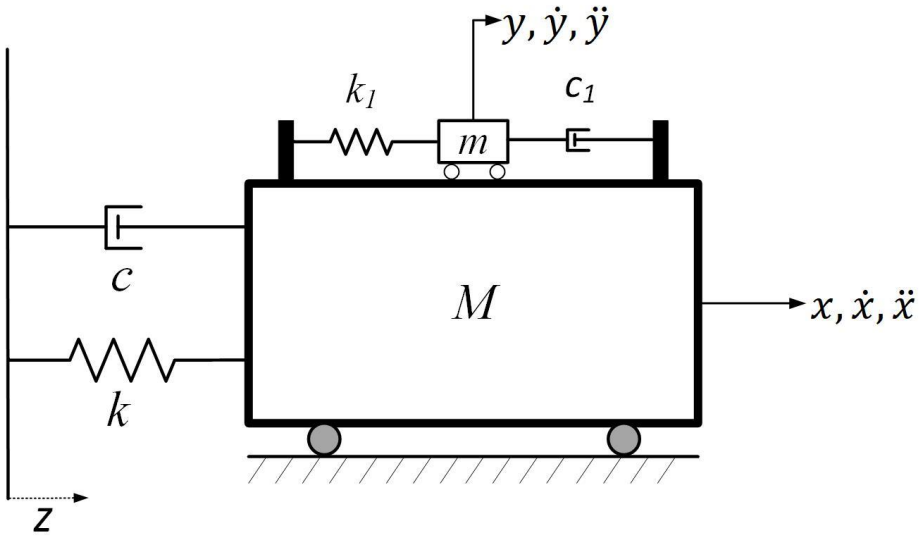

Fig. 3. Schematic model of tuned mass damper (TMD)

The equation of motion of primary and secondary mass might be written as,

$$M\ddot{x} + k(x - z) + k_1(x - y) + c(\dot{x} - \dot{z}) + c_1(\dot{x} - \dot{y}) = 0 \quad (9)$$

$$m\ddot{y} + k_1(y - x) + c_1(\dot{y} - \dot{x}) \quad (10)$$

TMD can be optimally tuned for maximum suppression of the resonant vibration of the primary mass *M*. The optimum frequency and damping ratios of the TMD can be derived and written as [41],

$$\gamma_{opt} = \frac{1}{1 + \mu_1} \quad (11)$$

$$\zeta_{opt} = \sqrt{\frac{3\mu_1}{8(1 + \mu_1)}} \quad (12)$$

where $\mu_1 = m/M$, $\omega = \sqrt{k/M}$, $\omega_a = \sqrt{(k_1/m)}$, $\gamma = \omega_a/\omega_n$, and $\zeta = c/\left(2\sqrt{mk_1}\right)$.

3. Experimental Rig

A prototype of the SMID as shown in Fig. 4a is manufactured and tested on a single degree of freedom (SDOF) structure to validate the numerical results. The experiment setup as shown in Fig. 4 consists of a primary mass, contactless displacement sensors, an exciter, and a data acquisition system connected to a computer. The primary system is a frame structure with two

steel beams acting as leaf springs of 1.5 mm thickness with an aluminium plate fixed on top of the springs.

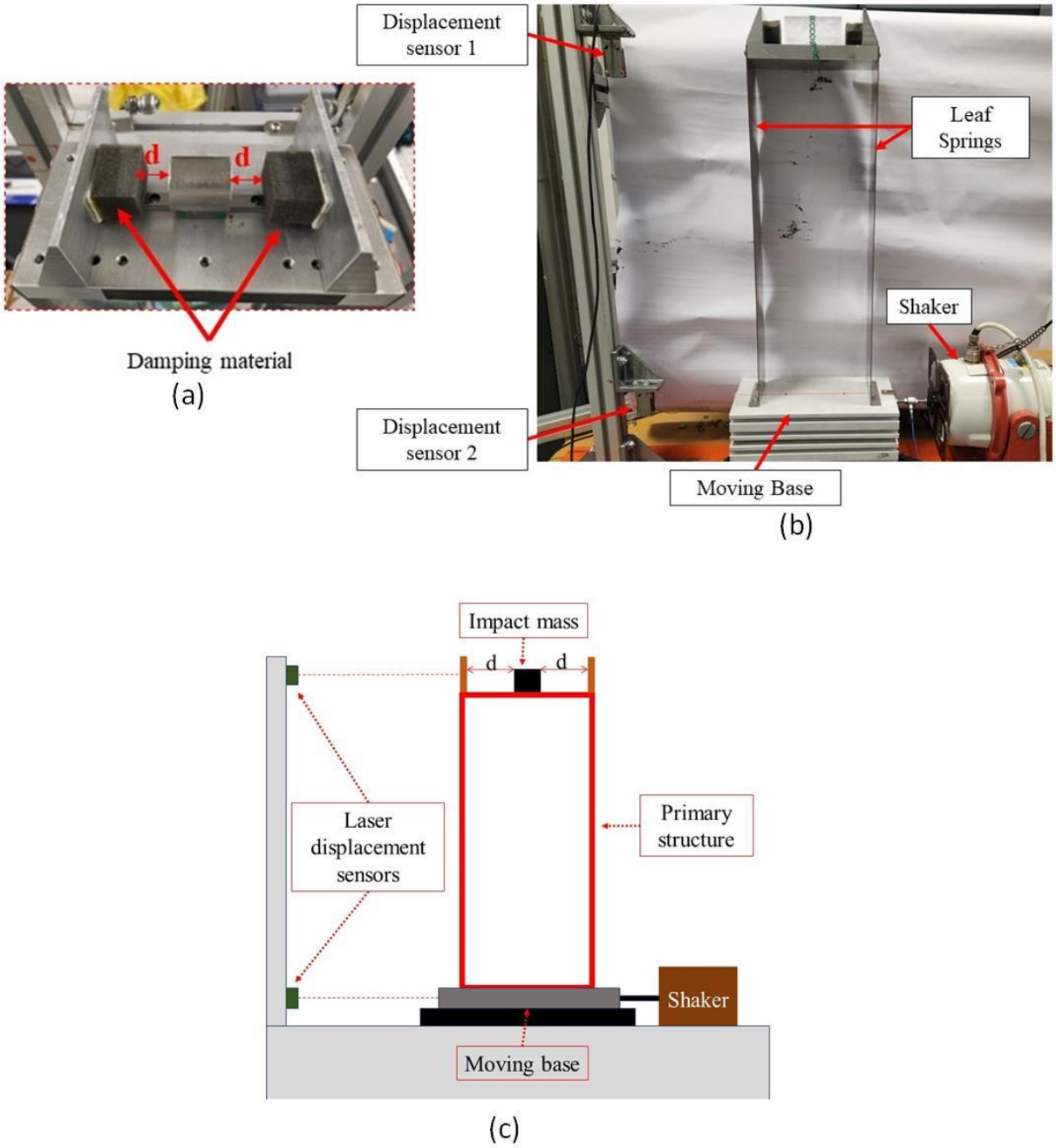

Fig. 4. A prototype of the single-degree-of-freedom structure and single-mass impact damper. (a) Single mass impact damper; (b) Experimental setup; (c) Sketch of experiments

The single-mass impact damper as shown in Fig. 4a consists of a cylindrical particle, which can slide on the top surface of the primary structure. Additionally, the impact surface in the SMID can be altered by changing the damping material to test the effect of the coefficient of restitution *e* on the damping performance of the SMID. Fig 4b shows the manufactured experiment rig and Fig 4c shows the sketch of the experimental setup for better understanding.

3.1. System's parameters identification

3.1.1. Primary Structure

It is assumed that the structure has no damping source other than the single-mass impact damper. However, there are many factors which add damping to the vibrating structure, such as air drag. Therefore, the free vibration tests of the primary structure are carried out without any external damping to determine the magnitude of structural damping present within the primary structure. The structure is provided with an initial displacement ($x_0 = 35$ mm) to initiate the free vibrations. The free vibration response is recorded and the logarithmic decrement method is used to determine the internal damping magnitude of the structure. Furthermore, performing a fast Fourier transform of the displacement data provides the natural frequency of the structure. The parameters of the primary structure are shown in Table 1.

Table 1. System parameters.

Parameter	Magnitude
Damping ratio (ζ)	0.0038
Natural frequency (f_n)	2.50 Hz
Primary mass (M)	1.61g

3.1.2. Single-mass impact damper

In the proposed numerical model of a single-mass impact damper, vibration damping to the primary structure is due to the energy dissipation and momentum exchange through impacts. The impact time is neglected in the simulations. Another assumption for this model is that the coefficient of restitution remains constant during the operation of the impact damper. Zero impact time may be justified with the hard impacts as it is a robust impact, and the time of contact is extremely short. However, a wide range of design parameters including the coefficient of restitution *e* is considered in this study to formulate a methodology for the optimal design of the SMID. In order to study the effect of the coefficient of restitution of the impact surfaces in the SMID on its damping performance, a smaller coefficient of restitution representing soft impacts in the SMID is also used in the tests by using a soft impact surface such as cushion foam. The soft impact surface has a much larger deformation than the hard surface during the impact and therefore a relatively larger contact time can be expected in such a case. In order to validate the assumptions, a few experiments are conducted to determine the contact time for soft and hard impact surfaces. Additionally, the coefficient of restitution of the soft impact surface of the SMID is determined with different velocities of the particle before and after impact.

The experimental measurement of contact time and coefficient of restitution is conducted by free fall experiments of the particle. A metallic particle is dropped from a known height. The particle rebounds after the impact with a soft or hard surface. The whole process is recorded with a high-speed camera (Sony RX100-M7) in slow motion (20x). The high-speed camera can record videos at 1000fps. The high frame rate increases the accuracy of the measurement as it can record the deformation of the impact surface of the SMID. The coefficient of restitution is defined as the ratio of velocity after and before each impact as,

$$e = \frac{v_f}{v_i} = \frac{\sqrt{2gh_f}}{\sqrt{2gh_i}} = \sqrt{\frac{h_f}{h_i}} \tag{13}$$

The video frames of the dropping and rebounce of the particle are carefully extracted from the video and processed in the CAD software to determine the ratio of final to initial height and contact duration. The measured contact time and coefficient of restitution for soft and hard materials are presented in Table 2.

Table 2. Contact time and average COR between different impact types

Impact nature	Contact Time (s)	Coefficient of restitution
Soft Impact	0.074	0.47
Hard Impact	0.011	0.82

It is shown that a soft impact takes approximately 6.72 times longer duration than a hard impact. The soft impact is produced by installing a cushioning foam (polyurethane foam) at the impact surface, while the hard impact is generated by using an aluminium impact surface in the SMID.

4. Results and discussions for free vibration response

4.1. Numerical simulations analysis

In this section, the performance of the single-mass impact damper (SMID) in free vibration damping is analyzed. Free vibrations may be initiated by an impulse force, or a swift seismic jolt to the dynamic system leading to an initial displacement, velocity or acceleration of the system. The free vibration response of an SDOF structure associated with a single-mass impact damper as shown in Fig. 1 is analyzed in this section. The equation of motion of the primary mass can be obtained from Equation (1) by setting $z(t) = 0$. The free vibration response of the mass *M* is simulated with an initial displacement of 35mm to the primary mass and the equations of motion, Eqs. (1) and (2), are solved by using Runge Kutta's fourth-order equation solver of MATLAB software. The vibration amplitudes of the primary mass *M* with the SMID of different

clearance, d/x_0, and coefficient of restitution, e, are simulated and plotted in Fig. 5. The free vibration amplitudes of the SDOF structure with TMD ($k_1 = 32.83$ N/m) with a similar mass ratio as SMID (mass ratio = 0.1) in Fig. 3 are also solved numerically and plotted in Fig. 5 for comparison. As shown in Fig. 5, the vibration amplitude of the primary mass *M* reduces very slowly if no TMD or SMID is installed to provide damping to its vibration. The SMID can damp the vibration of mass *M* much faster than the TMD. While the TMD provides a gradual reduction of the vibration amplitude of the mass *M*, the SMID has uneven damping at different cycles of vibration of the mass *M*. The SMID with a soft impact surface can damp down the vibration amplitude of mass *M* much faster than the SMID with a hard impact surface. The SMID of a larger clearance can damp down the vibration amplitude of mass *M* faster because the particle of the SMID can gain higher velocity before impact so the energy dissipation of the two masses during impact becomes more efficient.

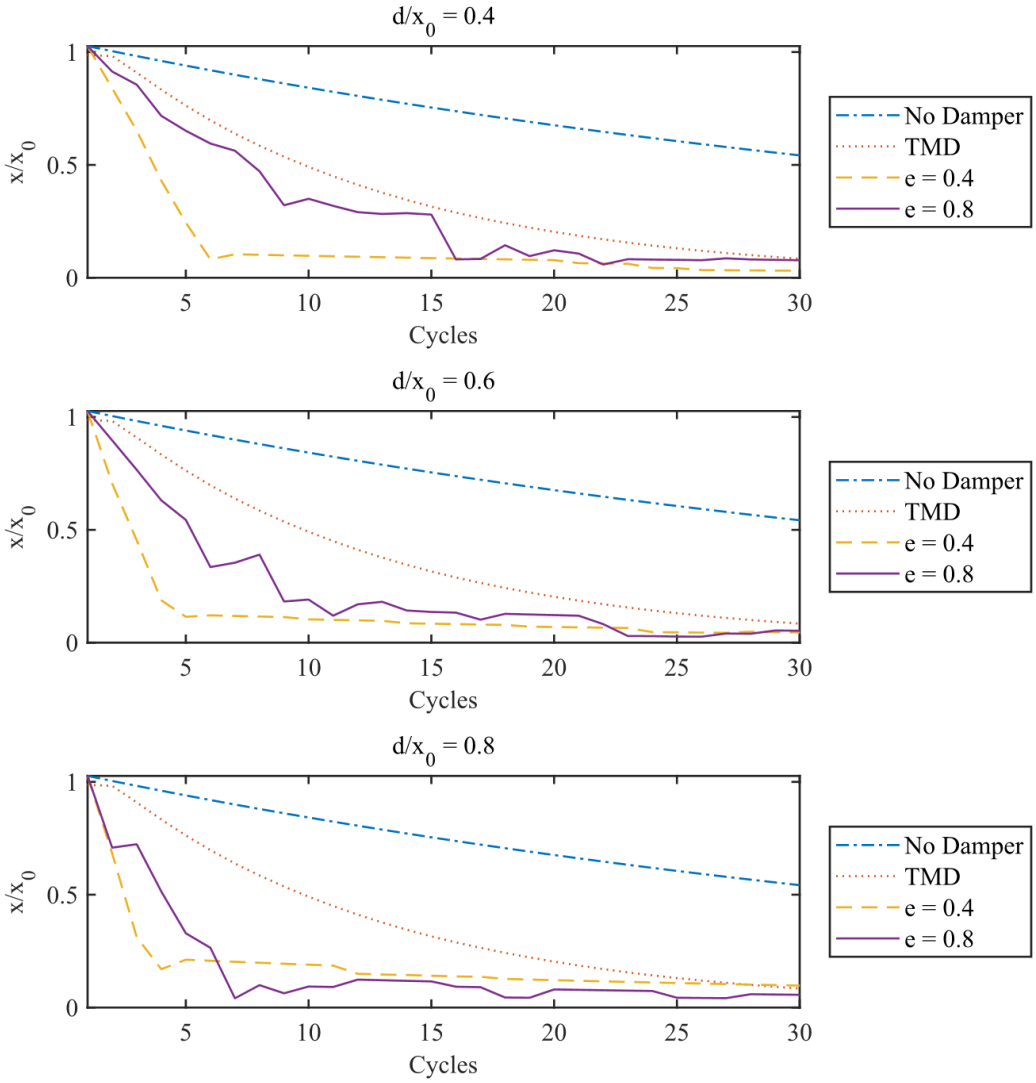

Fig. 5. Free vibrations response of the primary structure with frictionless single-mass impact damper; $\mu_i = 0$

It is worth noting that the velocity of the particle is of high importance in the single-mass impact damper. The velocity is directly affected by the internal friction present between the particle and primary mass. Therefore, studying the single-mass impact damper requires a sense of internal friction. Friction can not be neglected in most mechanical systems, therefore, further analysis of the response of the primary mass is accomplished by considering the internal friction of the SMID. Simulating the response of the primary structure with different magnitudes of the internal coefficient of friction of the SMID shows that it has a direct effect on the damping performance of the SMID, as shown in Fig. 6. It can be observed that the cases of zero and a very small amount of internal friction ($\mu_i = 0.05$) of the SMID show the best damping performance of SMID to reduce the free vibration amplitudes of the primary structure. Therefore, it is recommended to keep the internal friction of the SMID as low as possible in practice.

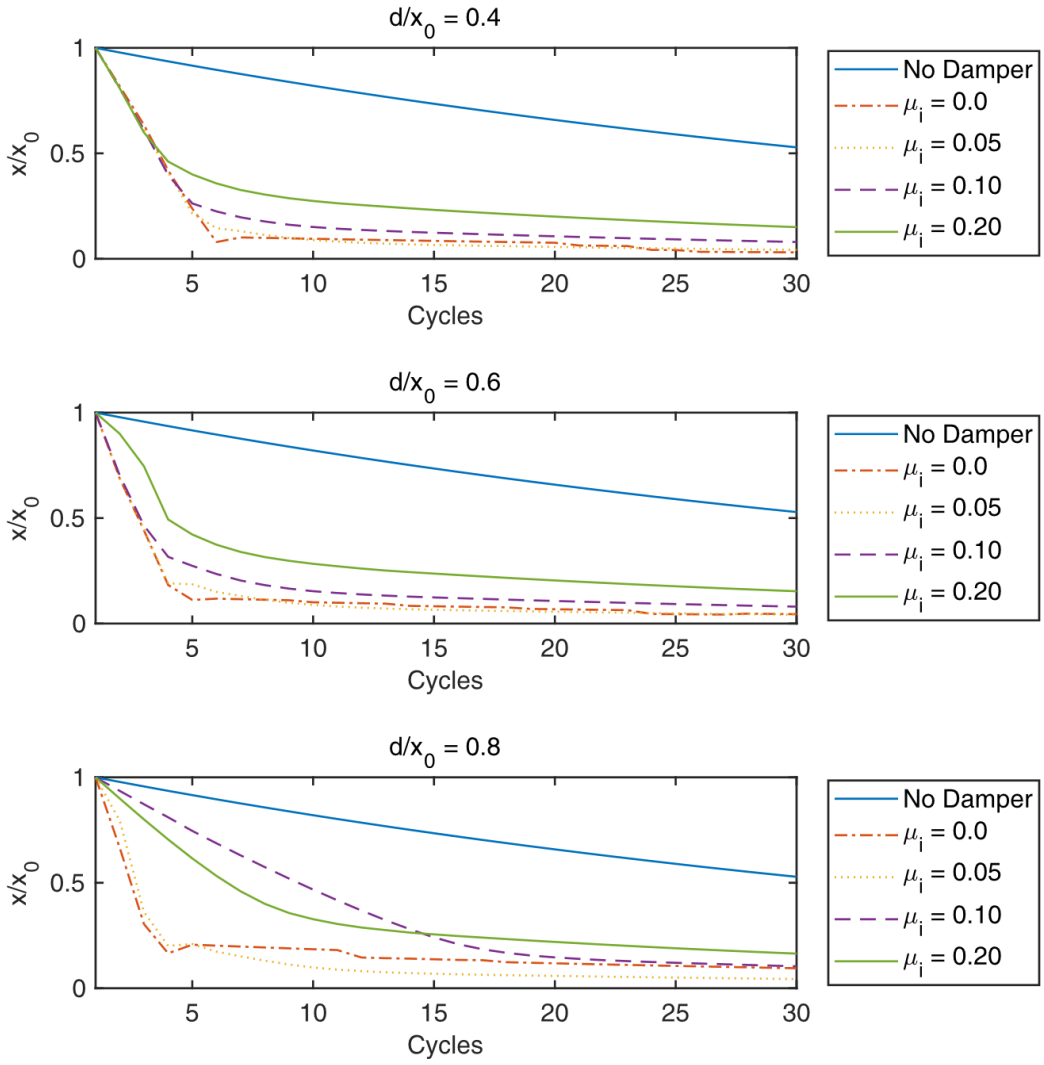

Fig. 6. Simulated free vibrations response of the primary structure with different internal coefficients of friction μ_i of the SMID, $e = 0.4$

4.1.1. Optimal Design Estimation

The overall influence of internal friction with various combinations of the design parameters of the SMID is analyzed in this section. Since the SMID has a non-uniform damping performance as discussed in the previous section, the root-mean-square (RMS) displacement magnitude of the first 30 cycles of the vibrations of the primary structure is calculated and plotted in Fig. 7for the analysis of its damping performance. RMS can represent the overall energy dissipation in the system, and it can be advantageous for systems with non-uniform damping [42, 43].

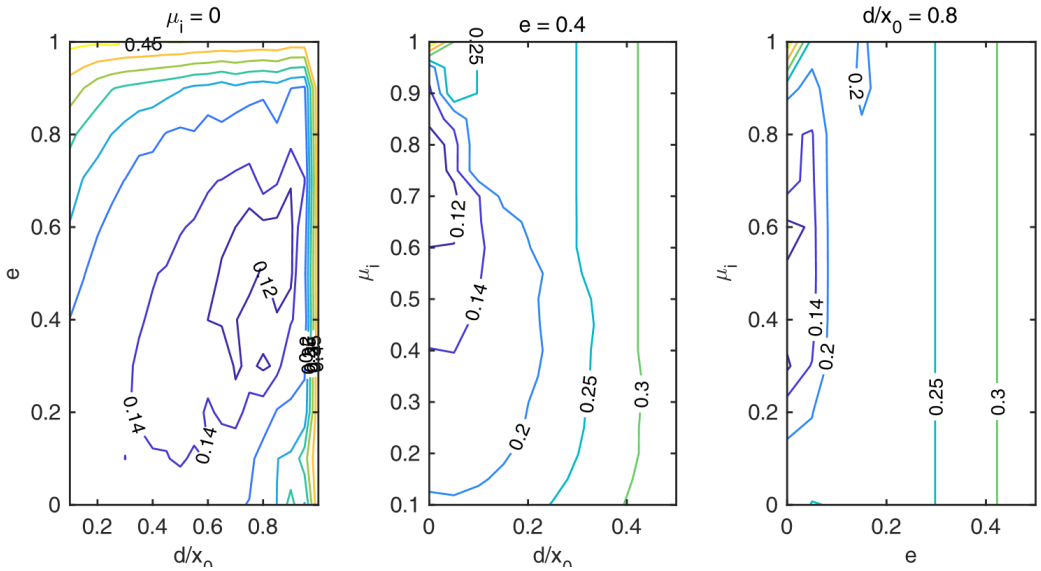

Fig. 7. RMS displacement of the SDOF structure under free vibrations with various combinations of design parameters of the single-mass impact damper. $\beta = 0.1$; (a) $\mu_i = 0$; (b) $e = 0.4$; (c) $d/x_0 = 0.8$.

As shown in Fig. 7a, the RMS displacement of the mass M becomes insensitive to the clearance magnitude d/x_0 when e is close to 1 because there is almost no energy dissipation by the impacts. Surprisingly, the lower magnitude of the coefficient of restitution e referring to the higher energy dissipation does not necessarily lead to better damping. Therefore, the momentum exchange through impacts is equally important for damping through SMID. Fig. 7a shows that there the minimum RMS displacement of the mass M exists at $e \approx 0.55$ and $d/x_0 \approx 0.85$. Therefore, determining the optimal values of the design parameters of the SMID for optimal energy dissipation and momentum exchange becomes vital.

The contours in Fig. 7b and Fig. 7c also show the variations of the RMS displacement magnitude with clearance magnitude along with internal friction, and coefficient of restitution combined with internal friction, respectively. The two graphs show a clear influence of internal friction on the adverse effect of damping performance of the SMID.

4.1.2. Experimental Validations

In this section, the experimental analysis is presented. The experiments are conducted for the free vibration response of the structure with different damper settings. The experimental model as shown in Fig. 4 can test a few sets of design parameters of the SMID including the clearance magnitude, the internal friction and the coefficient of restitution of the SMID. The optimal design assessment showed that the coefficient of restitution should be between 0.4 to 0.6. Therefore, the coefficient of restitution is obtained at 0.47 by installing a polyurethane (PU) foam on the surface of the stoppers of the SMID. The relative clearance magnitude can be changed to test different settings. Furthermore, a sliding mechanism with linear bearings is installed on the surface of the primary structure to minimize friction during the motion of the particle, as shown in Fig. 3. This mechanism ensures the sliding motion of the particle in compliance with the numerical model.

The relative clearance magnitude, d/x_0, is altered to test the different design combinations of the single-mass impact damper as well. The free vibration response of the structure is recorded by providing an initial displacement $(x_0 = 35\ \text{mm})$ to the structure. The normalized displacement of the primary structure with different clearance magnitudes is shown in Fig. 8. The results show that the smaller clearance magnitude can provide damping for a longer time, however, the damping is relatively lower due to the lesser energy of the particle because of the small clearance. On the other hand, a larger clearance magnitude provides larger damping in the first few cycles but the damping deteriorates quickly and extremely lower damping can be seen after a few cycles. Therefore, a relative clearance magnitude (d/x_0) of 0.75 performs better in terms of robust and longer-duration damping, which was suggested by the numerical analysis. Fig. 8b shows that there is a reasonable agreement between experiments and simulations and it shows that the damping performance of SMID depends significantly on the clearance magnitude and the relationship between these parameters is nonlinear.

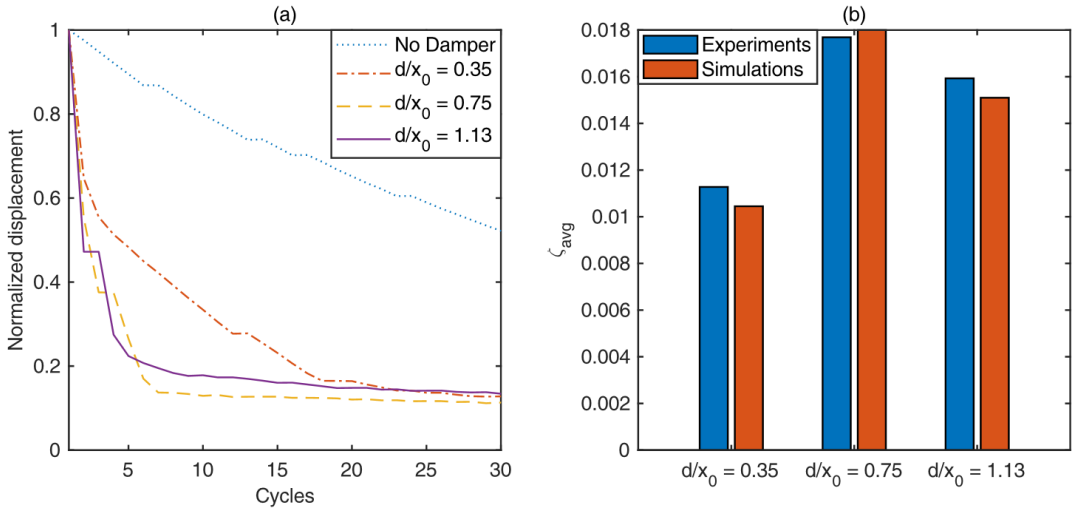

Fig. 8. (a) Free vibration response of the primary structure with different clearance magnitudes of SMID; (b) Comparison of average damping ratio with different clearance magnitudes

To test the effect of internal friction on the damping performance of the SMID, three mechanisms are designed to provide three different levels of internal friction. The coefficients of friction with different internal surfaces of the SMID are determined experimentally and they are listed in Table 3. The slider only refers to the rail train mechanism where a rail is fixed on the top surface and the particle is fixed on the corresponding train as shown in Fig. 4a. On the other hand, an acrylic tube is installed on the top of the primary mass as shown in Fig. 4b and the particle can slide on the surface of the acrylic tube without any sliding aid (rail-train). In such a case, the friction between the acrylic surface and the steel particle is larger than the rail-train mechanism. In order to further increase the friction, sandpaper (280cw) is fixed inside the acrylic tube and the particle can slide on the sandpaper with relatively larger friction.

The tested surfaces are fixed on an inclined plane of inclination angle θ in turn allowing the particle to slide down the tested surface. The sliding motions of the particle are recorded with the high-speed camera mentioned in Section 3.1.2. The time for the particle to reach the lowest end of the plate is recorded for each test surface for the determination of the acceleration of the particle in each case. Furthermore, a similar approach is used to determine the coefficient of friction for the slider as well. The coefficient of friction in each case is determined using Eq. 14 below.

$$\mu_i = \frac{g\sin(\theta) - a}{g\sin(\theta)} \tag{14}$$

Table 3. Coefficient of internal friction with different internal surfaces of the SMID.

Internal Surface	Coefficient of friction (μ_i)
Slider only	0.08
Without slider	0.18
Sandpaper (280cw)	0.25

The normalized displacement response according to the initial displacement of the primary structure with different internal friction magnitudes is presented in Fig. 9a. The results show that reducing internal friction improves vibration suppression in all tested combinations, verifying the results from numerical analysis.

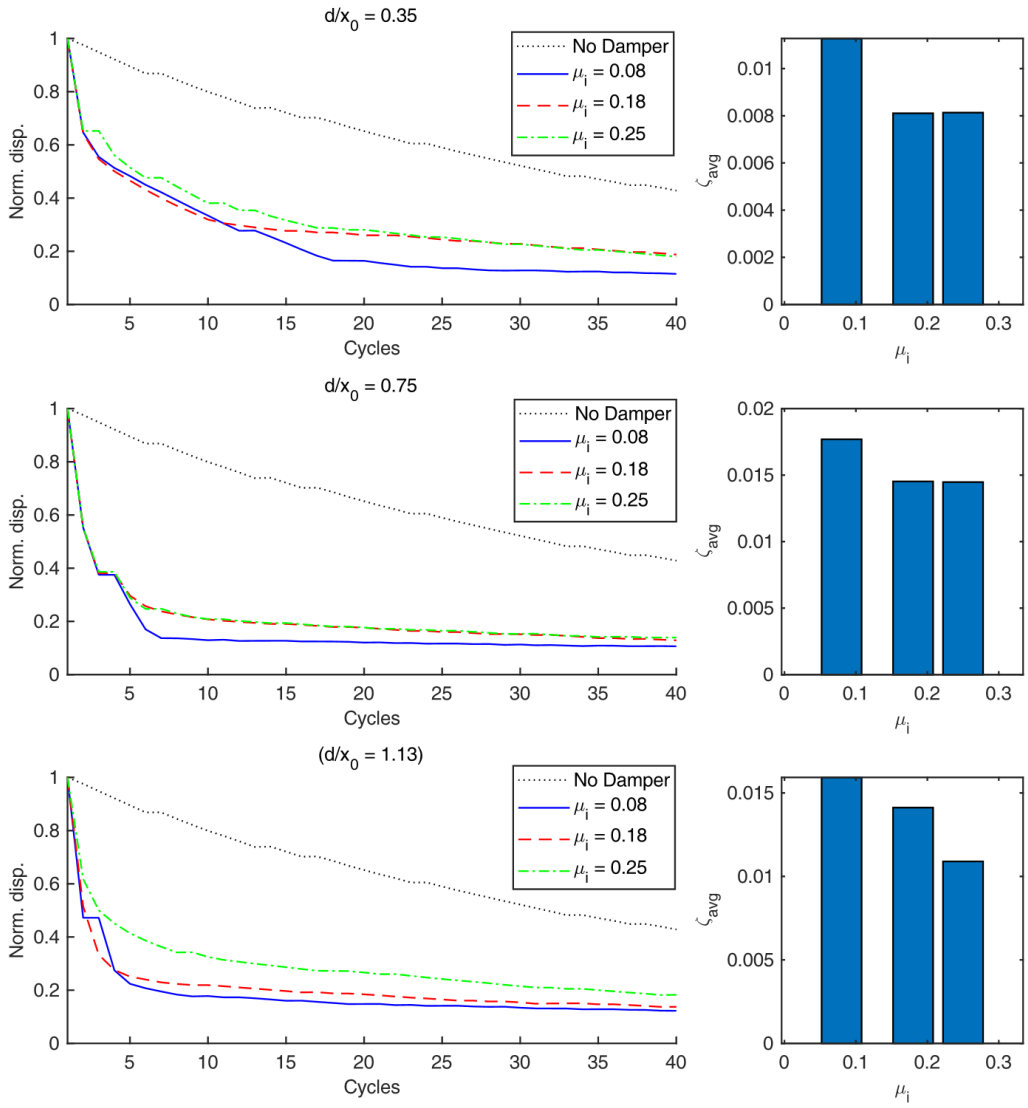

Fig. 9. Experimentally recorded normalized displacement of the primary structure with different internal friction magnitudes.

5. Results and discussion for forced vibration response

In this section, numerical and experimental analysis of a single-mass impact damper is conducted when the structure is experiencing harmonic excitations.

5.1. Numerical Analysis

The equations of motion of the primary structure and particle in Section 2 are solved numerically using the Runge-Kutta 4th-order method. Here $z(t) = Z\,sin(\omega t)$ is the harmonic base excitation, where Z is the amplitude and ω is the excitation frequency of the base motion. The damping performance of the SMID on the resonant vibration of the SDOF primary structure as shown in Fig. 1 can be observed from the simulation results in Fig. 10 for the response amplitudes of the primary mass M about its resonant frequency. The vibration amplitude of mass M in the frequency domain shows that the clearance to base motion amplitude, d/Z, has a large effect on the vibration amplitude of the SDOF primary structure.

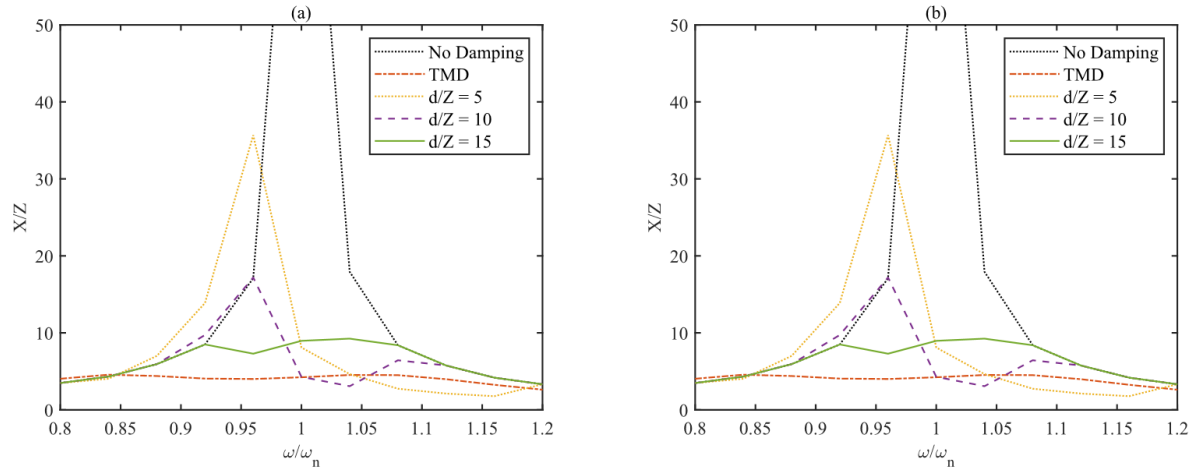

Fig. 10. Frequency response of the primary structure with different clearance to base motion amplitude. $e = 0.5$; (a) $Z = 3$ mm; (b) $Z = 30$ mm.

In addition, the response amplitude of the primary mass M is recorded for different magnitudes of base excitation. Fig. 10a shows the response of the structure for a base excitation magnitude of $Z = 3$ mm, while Fig. 10b shows the response of the structure for $Z = 30$ mm. Numerical results show that the clearance magnitude can be selected for any excitation amplitude if the ratio of d/Z remains constant.

As shown in Fig. 10, the clearance magnitude plays an important role similar to the free vibration analysis. The smaller clearance of the SMID leads to more impacts with low relative velocity, leading to lesser energy dissipation from SMID. The particle acts like an added mass to the

primary structure causing the lowering of the resonant frequency of the vibrating system. The frequency response of the primary structure with the TMD as shown in Fig. 3 is also simulated and plotted in Fig. 10 for comparison. It reveals that the single-mass impact damper cannot reduce the resonant amplitude of the primary mass as much as the optimized TMD. However, the optimum design of TMD is difficult to be achieved in practice because the optimized TMD requires both a precisely tuned frequency ratio and damping ratio for its operation. On the other hand, a single-mass impact damper is very simple to design and install. Unlike TMD, a single-mass impact damper can work for a structure with any natural frequency. Additionally, TMD is usually tuned for one frequency and it can be effective at that frequency only. Finally, a single-mass impact damper could be a very cost-effective solution for various vibration control problems. Therefore, a single-mass impact damper may be used when the application requires a cost-effective solution.

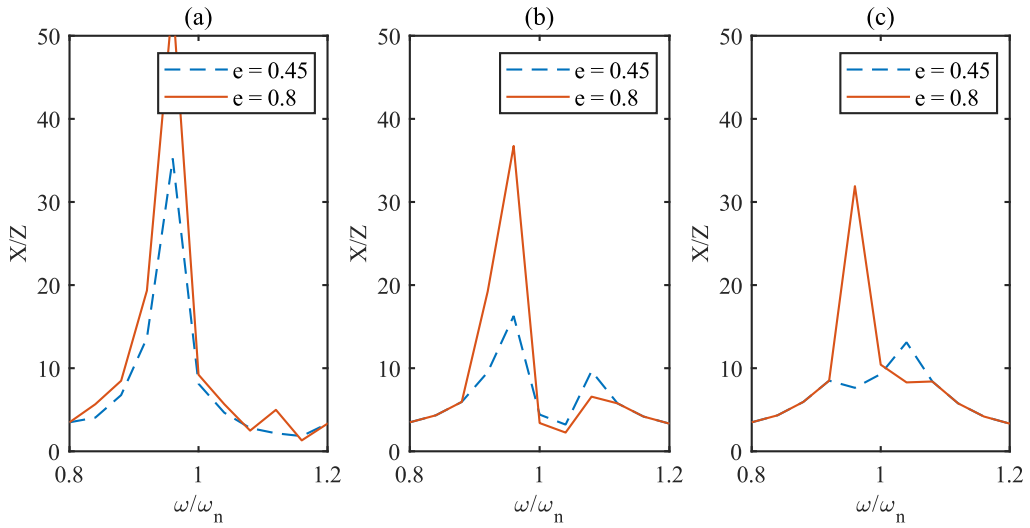

Fig. 11. Frequency response of the primary structure at resonance with single-mass impact damper; (a) $d/Z = 5$; (b) $d/Z = 10$; (c) $d/Z = 15$

The effect of the coefficient of restitution on the vibration amplitude of the primary mass *M* with difference clearance is shown in Fig. 11. The graphs in Fig. 11 show that the larger coefficient of restitution does not improve the performance of the single-mass impact damper. The analysis shows that an added mass (particle) requires an appropriate selection of design parameters (clearance, coefficient of restitution) for a controlled movement to achieve desirable damping, otherwise, an uncontrolled added mass to a vibrating structure may cause chaos and other nonlinear phenomena. Fig. 11a shows that the coefficient of restitution does not affect the damping too much when the clearance magnitude is small. Understandingly, the particle has very limited movement with a smaller clearance magnitude leading to excessive impacts with

low relative velocity. Hence, the energy dissipation and conservation of momentum are not significant with any magnitude of the coefficient of restitution. In addition, the coefficient of restitution begins influencing the damping performance as the clearance magnitude increases as shown in Figs. 11b and 11c. Therefore, it is necessary to understand the role of the coefficient of restitution in the design of a single-mass impact damper.

Besides the effectiveness of a single-mass impact damper over the resonance frequency of the structure, the chaotic response of the primary structure is another problem to analyse with a single-mass impact damper. The results with different design combinations of the single-mass impact dampers show different kinds of responses. A Poincaré map is a recurrence plot based on the state of the dynamic system in each cycle of vibration [44]. The Poincaré map of the primary structure is determined for various parameters to provide insight into the nature of displacement of the structure associated with the impact damper.

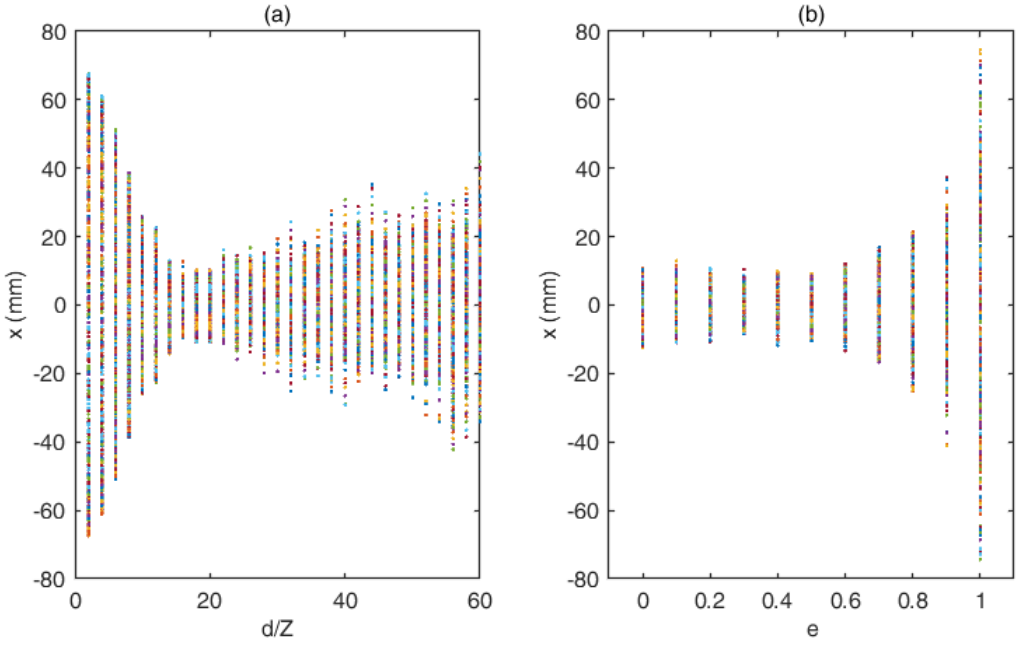

Fig. 12. Poincaré map of the primary structure with single-mass impact damper; (a) Relative clearance $e = 0.5$; (b) Coefficient of restitution, $d/Z = 14$

The Poincaré map is simulated for various magnitudes of relative clearance and coefficient of restitution, as shown in Fig. 12. The Poincaré map in Fig. 12a over different clearance levels shows that there will be different responses with altering clearance magnitude. Physically, clearance magnitude affects the velocity of the particle before each impact. Having a smaller clearance magnitude refers to the smaller velocity before impact and hence extremely low damping at smaller clearance magnitudes. In contrast, the larger clearance magnitude leads to a

higher velocity of particles that can benefit the damping through impacts, however, it aids the damping up to a certain extent. Having an extremely large clearance magnitude leads to a very high impact velocity, which may lead to the chaotic response of the primary mass as the particle strikes with a higher velocity during the vibrations. In addition, the coefficient of restitution below 0.7 shows a relatively consistent response of the structure at resonance in Fig. 12b. A larger coefficient of restitution refers to a smaller energy dissipation at impacts but more momentum exchange. Therefore, it is evident that a larger coefficient of restitution provides lesser damping and the particle and primary mass exchange momentum at each impact. Generally, the Poincaré map shows the clearance magnitude for a single-mass impact damper design is of high importance. Any value of the coefficient of restitution can be selected below 0.7 depending on the availability of materials and then a suitable clearance magnitude can be determined. Regarding the nature of the vibration response, it is vital to understand how the design parameters affect it.

5.2. Optimal design estimation

It can be concluded from the numerical analysis that there are numerous combinations of single-mass impact damper designs. It is challenging to represent the results for all combinations, therefore, contour plots are used to observe the change in response to different combinations. The contour plot shows the displacement ratio over various combination ranges of design parameters and the region displaying the minimum vibration amplitudes can be regarded as the optimal design combination. First of all, the contour plot for the internal friction combined with the coefficient of restitution (e) and the relative clearance magnitude (d/Z) is simulated and plotted in Fig. 13a and Fig. 13b respectively. The contour maps show that the steady-state amplitude of the primary structure increases with the increase in the internal friction level, therefore minimum internal friction is recommended for the optimum damping with a relative clearance magnitude between 14 to 17, and a coefficient of restitution between 0 to 0.5.

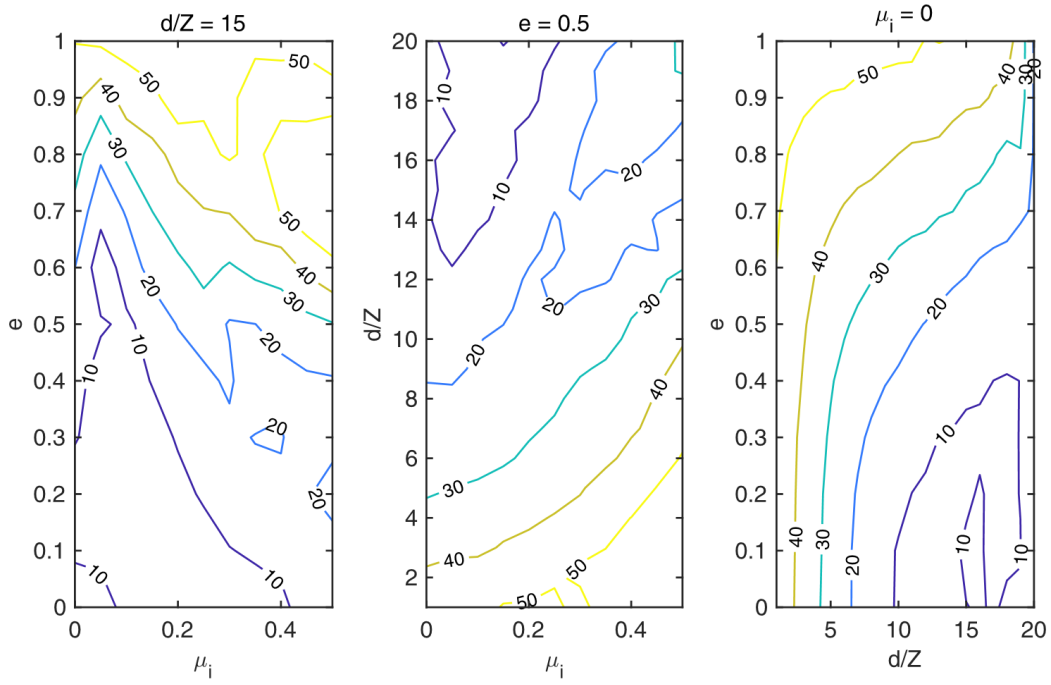

Fig. 13. Steady-state amplitude maps of the SDOF structure at resonance for optimal design estimation; (a) $d/Z = 15$; (b) $e = 0.5$; (c) $\mu_i = 0$.

It is understood that internal friction should be minimized for optimal performance of a single-mass impact damper. Therefore, a general optimal design combination can be determined by a contour plot between relative clearance magnitude and coefficient of restitution as shown in Fig. 13c. The contour shows that a very small clearance and large restitution coefficient have little effect on energy dissipation of the primary mass *M*. Additionally, a region where the clearance magnitude is between 10 to 16 and the restitution coefficient is 0 to 0.5 aids the damping performance. The design parameters selected within this region can maximize energy dissipation.

5.3. Experimental Validations

In this section, the optimal design combinations concluded from the numerical analysis are validated experimentally. The experimental model described in Section 3 is used to record the vibrations of the SDOF structure with different parameters of a single-mass impact damper. The primary structure is fixed on a base which is excited through a shaker. There are two laser displacement sensors placed within the experiment setup. One displacement sensor records the displacement of the primary mass while the second record the displacement of the base simultaneously.

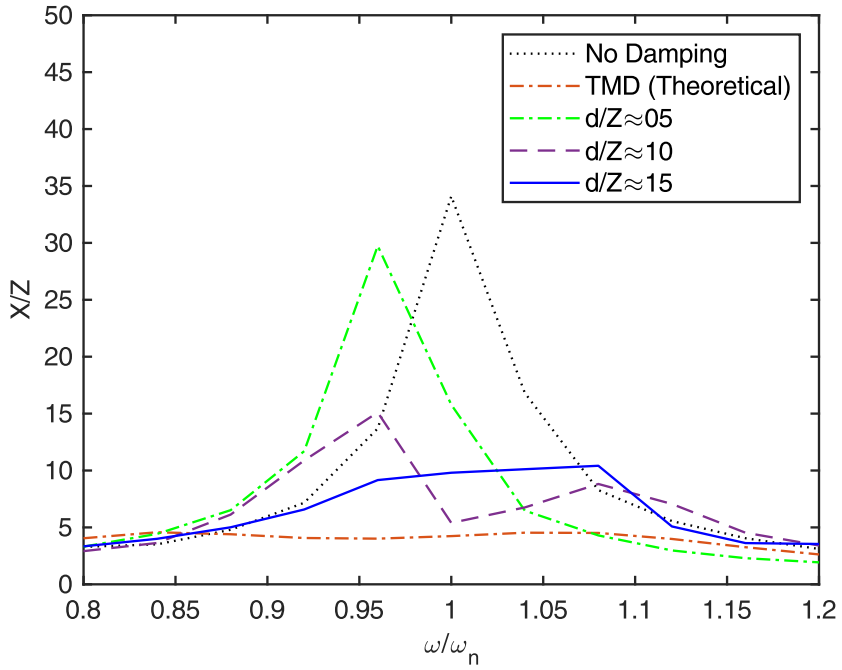

Fig. 14. Displacement ratio of the primary mass.

Commonly used sweep sine tests can no longer be valid for SMID because of the non-uniform damping. Therefore, a sweep sine test for SMID requires exciting the structure at a set of frequencies including the resonance frequency separately and using each excitation frequency displacement data to form a sweep sine plot. Due to the limitations of the experimental model, the experiments are performed for three different clearance magnitudes by keeping the $e \approx 0.45$ and $e \approx 0.8$ to validate the numerical results. The frequency response curves of the primary structures are plotted in Fig. 14 and it shows a similar trend to the numerical prediction in Section 5.1.1. The clearance magnitude plays an important role in the damping performance of SMID. A smaller clearance $(d/Z \approx 5)$ leads to extremely lower damping as there is not enough room for the particle to generate impacts with any significant velocity.

In order to estimate the validity of numerical simulations, the maximum amplitude ratio with different clearance magnitudes is compared in Table 4. It is well established now that there are complicated nonlinear phenomena involved with impact damping, therefore, it is quite challenging to include every phenomenon in the numerical model. However, the results show that there is good agreement with numerical and experimental data and the conclusions for optimal design drawn from numerical simulations are valid in experimental results.

Table 4. Comparison of maximum amplitude ratio determined from experiments and numerical simulations with different clearance magnitudes

	$d/Z \approx= 5$	$d/Z \approx= 10$	$d/Z \approx= 15$
$\max(X/Z)$ (Simulation)	35.6	17.2	9.3
$\max(X/Z)$ (Experiment)	29.7	15.1	10.4

The dimensionless displacements of the primary structure with different magnitudes of coefficient of restitution are measured and plotted in Fig. 15. It shows that the coefficient of restitution becomes increasingly effective in damping as the clearance magnitude is increased.

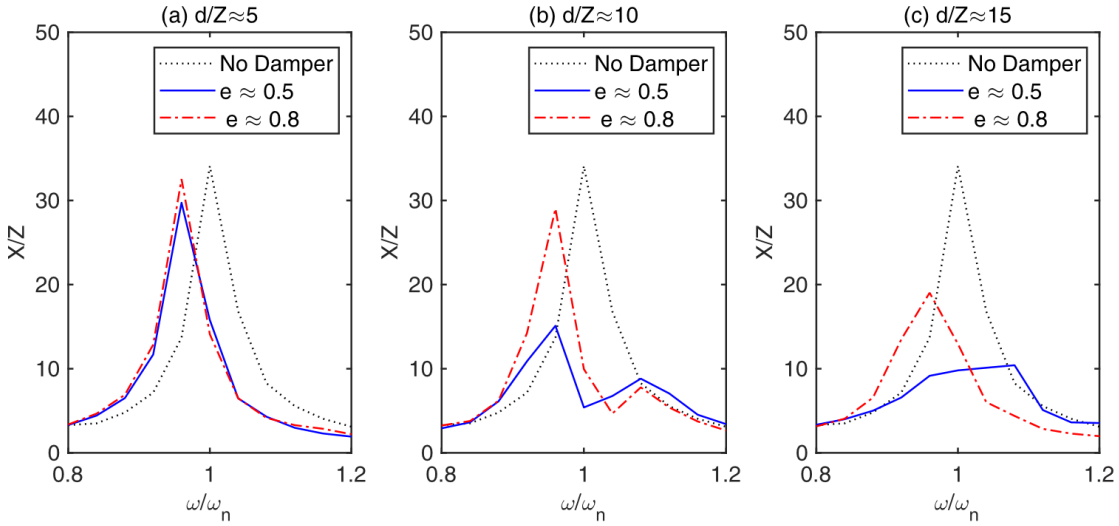

Fig. 15. Displacement of the primary structure with different magnitudes of coefficient of restitution.

Fig. 15a shows that the coefficient of restitution has almost no influence on the displacement of the primary structure with a clearance magnitude relatively smaller. However, the coefficient of restitution has a significant influence as the clearance magnitude is increased as shown in Figs. 15b and 15c. The graphs in Fig. 15 show that the single-mass impact damper with a larger clearance magnitude and the lower coefficient of restitution (e = 0.5) has the best damping performance.

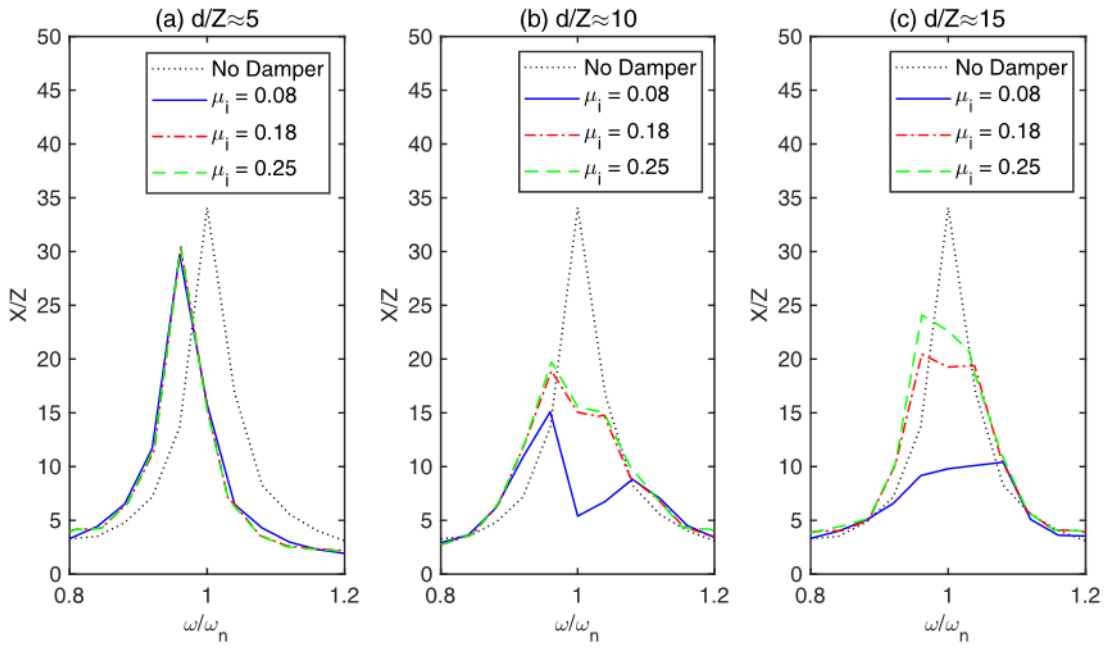

Fig. 16. Displacement of the primary structure with different levels of internal friction.

Fig. 16 compares the vibration amplitude with different levels of internal friction of the SMID. When the clearance magnitude is smaller, the internal friction has a lesser influence on the vibration amplitude (Fig. 16a). However, the influence of internal friction is significant as the clearance magnitude is increased (Fig. 16b and Fig. 16c). Overall, the results show that the increased internal friction reduces the damping provided by the SMID and increases the vibration amplitude of the primary SDOF structure.

6. Conclusion

This study presents a numerical approach for designing a single-mass impact damper (SMID) and establishes a methodology for optimizing its performance. A numerical model is developed to predict the performance of SMID under various design combinations. Additionally, the numerical model is modified to analyze the impact of internal friction on the SMID's performance. Incorporating internal friction in the simulations leads to results that closely match the experimental results. Furthermore, an experimental rig is fabricated based on the conclusions drawn from the numerical analysis. The experimental results validate the numerical approach and an optimal design methodology for SMID is formulated. The following conclusions are drawn based on the results obtained:

1. Internal friction in the SMID reduces the kinetic energy of particles, resulting in less significant impacts. The numerical and experimental results demonstrate that larger

friction magnitudes lead to lower damping in free and forced vibrations. Therefore, minimizing internal friction is recommended for optimal SMID performance.

2. Analyzing a large data set of vibration amplitude over a wide range of design combinations shows that the optimal design of SMID exists for any specific excitation. For the best performance, SMID should have a relative clearance magnitude, d/Z, between 14 to 18, where Z is the amplitude of base excitations, and the coefficient of restitution, e, is between 0 to 0.5. In free vibrations, the relative clearance magnitude, d/x_o, should be between 0.7 to 0.9, and restitution should be between 0.4 to 0.6 for optimal damping. The experimental results validate the conclusions drawn from the numerical analysis.

3. An uncontrolled mass (particle) may result in chaotic vibration patterns during the primary mass's vibration. Therefore, the Poincaré map is determined to identify a range of design parameters that show the regions where a relatively steady response is observed. The map indicates that selecting the design parameters correctly leads to a steady response, but a chaotic response is possible if a SMID is designed without proper understanding.

4. Comparing the optimized SMID to an optimized TMD shows that SMID can reduce the free vibration of the SDOF primary system faster than the optimized TMD but it is worse than the optimized TMD in suppressing the resonant forced vibration amplitude of the primary system. However, the SMID has the advantages of lower cost and easier installation than TMD, it may be a good choice for some vibration control applications.

The understanding of SMID is still in the preliminary stages, and its practical applications in structural vibration control are limited. This study demonstrates that SMID can be a tempting choice over other passive technologies and provides a simple yet effective solution.

Acknowledgement.

The authors would like to acknowledge The Hong Kong Polytechnic University for the funding support (Project number: 20031135r).

Conflict of interest:

The authors declare that they have no conflict of interest.

Data Availability

The datasets generated and analyzed during the current study are available from the corresponding author upon reasonable request.

References

[1] L. Gagnon, M. Morandini, G.L. Ghiringhelli, A review of particle damping modeling and testing, Journal of Sound and Vibration, 459 (2019).

[2] M. Żurawski, C. Graczykowski, R. Zalewski, The prototype, mathematical model, sensitivity analysis and preliminary control strategy for Adaptive Tuned Particle Impact Damper, Journal of Sound and Vibration, (2023) 117799.

[3] B.-s. Wang, H.-x. He, S.-t. Cheng, Y.-f. Chen, Experimental and optimization analysis of a multiple unidirectional single-particle damper, Journal of Sound and Vibration, 553 (2023) 117664.

[4] B. Wang, H. Wang, Z. He, D. Liu, P. Pan, Test and analysis of multi-cavity particle damper for vertical vibration control of pipeline structures, Eng Struct, 281 (2023) 115744.

[5] Y. Harduf, E. Setter, M. Feldman, I. Bucher, Modeling additively-manufactured particle dampers as a 2DOF frictional system, Mechanical Systems and Signal Processing, 187 (2023) 109928.

[6] M.A. Akbar, W.-O. Wong, E. Rustighi, A Hybrid Damper with Tunable Particle Impact Damping and Coulomb Friction, Machines, 11 (2023) 545.

[7] Y. Wei-ming, W. Bao-shun, H. Hao-xiang, Research of mechanical model of particle damper with friction effect and its experimental verification, Journal of Sound and Vibration, 460 (2019).

[8] Q. Wang, D. Dan, A simplified modeling method for multi-particle damper: Validation and application in energy dissipation analysis, Journal of Sound and Vibration, 517 (2022).

[9] G.R. Tomlinson, D. Pritchard, R. Wareing, Damping characteristics of particle dampers - some preliminary results, P I Mech Eng C-J Mec, 215 (2001) 253-257.

[10] M. Saeki, Impact damping with granular materials in a horizontally vibrating system, Journal of Sound and Vibration, 251 (2002) 153-161.

[11] Z. Lu, K. Li, Y. Zhou, Comparative Studies on Structures with a Tuned Mass Damper and a Particle Damper, Journal of Aerospace Engineering, 31 (2018).

[12] Z.W. Xu, M.Y. Wang, T.N. Chen, Particle damping for passive vibration suppression: numerical modelling and experimental investigation, Journal of Sound and Vibration, 279 (2005) 1097-1120.

[13] R. Ibrahim, Vibro-impact Dynamics: Modeling, Mapping and Applications, Springer-Verlag, Berlin Heidelberg, 2009.

[14] Z. Lu, X.L. Lu, H.J. Jiang, S.F. Masri, Discrete element method simulation and experimental validation of particle damper system, Eng Computation, 31 (2014) 810-823.

[15] G. Michon, A. Almajid, G. Aridon, Soft hollow particle damping identification in honeycomb structures, Journal of Sound and Vibration, 332 (2013) 536-544.

[16] X.Y. Wang, X.D. Liu, Y.C. Shan, T. He, Design, simulation and experiment of particle dampers attached to a precision instrument in spacecraft, Journal of Vibroengineering, 17 (2015) 1605-1614.

[17] Z.W. Xu, M.Y. Wang, T.N. Chen, A particle damper for vibration and noise reduction, Journal of Sound and Vibration, 270 (2004) 1033-1040.

[18] A.E. Diniz, W.T.A. da Silva, D.I. Suyama, R. Pederiva, M.V. Albuquerque, Evaluating the use of a new type of impact damper for internal turning tool bar in deep holes, Int J Adv Manuf Tech, 101 (2019) 1375-1390.

[19] B. Xian-Ming, S. Binoy Milan, M.K. Leon, Q.J. Wang, Q.S. Randall, Particle dynamics simulations of a piston-based particle damper, Powder Technology, (2009).

[20] J. Wang, M. Juan, S. Yang, D. Zhang, Z. Zhang, J. Jin, T. Yu, Experimental Investigation of the Vibration Reduction of the Pipeline System with a Particle Impact Damper under Random Excitation, Applied Sciences, 13 (2023) 618.

[21] Y. Zhang, J. Cheng, W. Xu, C. Wang, J. Liu, Y. Li, S. Yang, Particle Damping Vibration Absorber and Its Application in Underwater Ship, Journal of Vibration Engineering & Technologies, (2022).

[22] A. Papalou, E. Strepelias, D. Roubien, S. Bousias, T. Triantafillou, Seismic protection of monuments using particle dampers in multi-drum columns, Soil Dynamics and Earthquake Engineering, 77 (2015) 360-368.

[23] P. Lieber, D.P. Jensen, An Acceleration Damper: Development, Design, and Some Applications, Transactions of the American Society of Mechanical Engineers, 67 (1945) 523-530.

[24] C. Grubin, On the Theory of the Acceleration Damper, Journal of Applied Mechanics, 23 (1965) 373-378.

[25] S.F. Masri, General Motion of Impact Dampers, Journal of the Acoustical Society of America, 47 (1970) 229-&.

[26] M. Sami Faiz, Analytical and experimental studies of impact dampers, (1965).

[27] K.N. Li, A.P. Darby, A buffered impact damper for multi-degree-of-freedom structural control, Earthquake Engineering & Structural Dynamics, 37 (2008) 1491-1510.

[28] K. Li, A.P. Darby, Experiments on the effect of an impact damper on a multiple-degree-of-freedom system, Journal of Vibration and Control, 12 (2006) 445-464.

[29] H. Safaeifar, A. Farshidianfar, Experimental and analytical investigation of impact dampers in free vibration reduction with coulomb friction, Noise & Vibration Worldwide, 53 (2021) 91-103.

[30] Y.Q. Yang, X. Wang, Investigation into the linear velocity response of cantilever beam embedded with impact damper, Journal of Vibration and Control, 25 (2019) 1365-1378.

[31] M.R. Duncan, C.R. Wassgren, C.M. Krousgrill, The damping performance of a single particle impact damper, Journal of Sound and Vibration, 286 (2005) 123-144.

[32] Z. Lu, Z.X. Wang, S.F. Masri, X.L. Lu, Particle impact dampers: Past, present, and future, Structural Control & Health Monitoring, 25 (2018).

[33] N. Meyer, R. Seifried, Damping prediction of particle dampers for structures under forced vibration using effective fields, Granular Matter, 23 (2021).

[34] T. Ehlers, S. Tatzko, J. Wallaschek, R. Lachmayer, Design of particle dampers for additive manufacturing, Additive Manufacturing, 38 (2021).

[35] H. Ye, Y.R. Wang, B. Liu, X.H. Jiang, Experimental Study on the Damping Effect of Multi-Unit Particle Dampers Applied to Bracket Structure, Appl Sci-Basel, 9 (2019).

[36] C. Wong, J. Rongong, Control of Particle Damper Nonlinearity, Aiaa Journal, 47 (2009) 953-960.

[37] H. He, B. Wang, W. Yan, Mechanical Model and Optimization Analysis of Multiple Unidirectional Single-Particle Damper, Journal of Engineering Mechanics, 147 (2021).

[38] X.H. Huang, W.B. Xu, J. Wang, W.M. Yan, Y.J. Chen, Equivalent model of a multi-particle damper considering particle rolling and its analytical solution, Structural Control & Health Monitoring, 28 (2021).

[39] Z. Lu, X. Lu, S.F. Masri, Studies of the performance of particle dampers under dynamic loads, Journal of Sound and Vibration, 329 (2010) 5415-5433.

[40] C.N. Bapat, S. Seshadri, Single unit impact damper in free and forced vibration, J Sound Vib, (1985).

[41] W.O. Wong, Optimal design of a hysteretic vibration absorber using fixed-points theory, J Acoust Soc Am, 139 (2016) 3110.

[42] M.U. Shah, M. Usman, An experimental study of tuned liquid column damper controlled multi-degree of freedom structure subject to harmonic and seismic excitations, PLOS ONE, 17 (2022) e0269910.

[43] Z. Zhao, Q. Chen, R. Zhang, C. Pan, Y. Jiang, Energy dissipation mechanism of inerter systems, Int J Mech Sci, 184 (2020) 105845.

[44] M.W. Hirsch, S. Smale, R.L. Devaney, 10 - Closed Orbits and Limit Sets, in: M.W. Hirsch, S. Smale, R.L. Devaney (Eds.) Differential Equations, Dynamical Systems, and an Introduction to Chaos (Third Edition), Academic Press, Boston, 2013, pp. 213-232.